Mon. Not. R. Astron. Soc. **000**, 1–?? (2012) Printed 20 May 2014 (MN LATEX style file v2.2)

The structure of Abell 1351: a bimodal galaxy cluster with peculiar diffuse radio emission

R. Barrena[1,2⋆], M. Girardi[3,4], W. Boschin[5], S. De Grandi[6], M. Rossetti[7,8]
[1] *Instituto de Astrofísica de Canarias, C/Vía Láctea s/n, E-38205 La Laguna (Tenerife), Spain*
[2] *Departamento de Astrofísica, Univ. de La Laguna, Av. del Astrofísico Francisco Sánchez s/n, E-38205 La Laguna (Tenerife), Spain*
[3] *Dipartimento di Fisica dell'Università degli Studi di Trieste - Sezione di Astronomia, via Tiepolo 11, I-34143 Trieste, Italy*
[4] *INAF - Osservatorio Astronomico di Trieste, via Tiepolo 11, I-34143 Trieste, Italy*
[5] *Fundación Galileo Galilei - INAF (Telescopio Nazionale Galileo), Rambla J. A. Fernández Pérez 7, E-38712 Breña Baja (La Palma), Spain*
[6] *INAF, Osservatorio Astronomico di Brera, via E. Bianchi 46, 23807, Merate (LC), Italy*
[7] *Dipartimento di Fisica dell'Università degli Studi di Milano, via Celoria 16, I-20133, Milan, Italy*
[8] *IASF-Milano, INAF, via Bassini 15, Milan 20133, Italy*

arXiv:1405.4707v1 [astro-ph.GA] 19 May 2014

Accepted DATE. Received DATE; in original form DATE

ABSTRACT

We aim to review the internal structure and dynamics of the Abell 1351 cluster, shown to host a radio halo with a quite irregular shape. Our analysis is based on radial velocity data for 135 galaxies obtained at the Telescopio Nazionale Galileo. We combine galaxy velocities and positions to select 95 cluster galaxy members and analyse the internal dynamics of the whole cluster. We also examine X-ray data retrieved from *Chandra* and *XMM* archives. We measure the cluster redshift, $\langle z \rangle = 0.325$, the line-of-sight (LOS) velocity dispersion, $\sigma_{\rm V} \sim 1500$ km s^{-1}, and the X-ray temperature, $kT \sim 9$ keV. From both X-ray and optical data independently, we estimate a large cluster mass, in the 1–4 $\times 10^{15}$ h_{70}^{-1} $M_{\odot}$ range. We attribute the extremely high value of $\sigma_{\rm V}$ to the bimodality in the velocity distribution. We find evidence of a significant velocity gradient and optical 3D substructure. The X-ray analysis also shows many features in favour of a complex cluster structure, probably supporting an ongoing merger of substructures in Abell 1351. The observational scenario agrees with the presence of two main subclusters in the northern region, each with its brightest galaxy (BCG1 and BCG2), detected as the two most important X-ray substructures with a rest-frame LOS velocity difference of $\Delta V_{\rm rf} \sim 2500$ km s^{-1}and probably being in large part aligned with the LOS. We conclude that Abell 1351 is a massive merging cluster. The details of the cluster structure allow us to interpret the quite asymmetric radio halo as a 'normal' halo plus a southern relic, strongly supporting a previous suggestion based only on inspection of radio and preliminary X-ray data.

Key words: Galaxies: clusters: general. Galaxies: cluster: individual.

1 INTRODUCTION

Very few galaxy clusters show powerful diffuse radio emission on a large scale. In general, this emission may be classified as 'radio haloes' and 'radio relics'. In the first case, the emission presents a compact morphology and comes from central cluster regions, while 'relics' are located in the peripheral zones (Ferrari et al. 2008; Giovannini et al. 2002; Feretti et al. 2012; Venturi 2011). The synchrotron origin of this radio emission demonstrates the presence of large-scale magnetic fields and relativistic particles distributed throughout the whole cluster. Today, cluster mergers are accepted as the most suitable scenarios proposed to supply enough energy for accelerating electrons to relativistic velocities and for magnetic field amplification.

In this framework, radio relics seem to be directly linked with merger shocks (Hoeft et al. 2004; Ensslin & Gopal-Krishna 2001; Roettiger et al. 1999; Ensslin et al. 1998). On the other hand, the remaining turbulence after cluster collision has been proposed as one of the most important mechanisms to produce giant radio haloes (Brunetti et al. 2001, 2009). Nevertheless, the precise mechanism for generating powerful radio haloes in clusters is still debated. In fact, there are two main theoretical approaches to the problem: re-acceleration vs. hadronic models (Brunetti et al. 2009 and references therein).

⋆ E-mail: rbarrena@iac.es

© 2012 RAS

Traditionally, the dynamical state of clusters with diffuse radio emission is studied using X-ray observations. Moreover, all statistical analyses on properties of radio emission are derived in general from X-ray data (Rossetti et al. 2011; Cassano et al. 2010; Buote 2002; Schuecker et al. 2001), and consist basically of temperature and luminosity (see e.g. Giovannini et al. 2002, and references therein). In fact, simulations based on turbulent re-acceleration models fit the observed radio haloes reasonably well (Cassano et al. 2006). Following the same line, Govoni et al. (2001) also find very good agreement between X-ray and radio emission when comparing, point by point, their respective surface brightnesses. Furthermore, Basu (2012) reports no evidence of bimodality in the radio-power–integrated SZ effect diagram whereas, on the contrary, Brunetti et al. (2007) find a bimodal distribution in the radio-power–X-ray luminosity plane. This controversy highlights the need to investigate the nature of radio haloes using other research techniques in addition to X-ray data.

The information on cluster members retrieved by radial velocities is an excellent way to study the kinematics and dynamics of mergers in clusters (Girardi & Biviano 2002). This technique allows us to detect cluster substructures by distinguishing pre- and post-merging groups, thus making it possible to disentangle the dynamics of ongoing mergers and remnants. Moreover, optical data complement and add information to X-ray because, during a collision, the ICM and galactic component respond on different timescales. Numerical simulations by Roettiger et al. (1997) clearly support this fact, hence the importance of combining optical and X-ray data to study the interactions of different cluster constituents. This is also the technique carried out by the MUSIC (MUlti-Wavelength Sample of Interacting Clusters) project (Maurogordato et al. 2011) to study merging scenarios.

In the context described above, we are conducting an intensive observational and data analysis programme to study the internal dynamics of clusters with diffuse radio emission by using member galaxies (DARC – Dynamical Analysis of Radio Clusters – project, see Girardi et al. 2010.[1]) As part of an ongoing programme to investigate the presence in complex X-ray cluster systems of halo emission from the sub-clusters in the merger, we have carried out a detailed and intensive study of the cluster Abell 1351 (hereafter A1351), also known as MACS J1142.4+5831. A1351 is a rich, X-ray luminous cluster: Abell richness class = 2 (Abell et al. 1989); $L_{\rm X}$(0.1–2.4 keV) = $8.31{\times}10^{44}\ h_{50}^{-2}$ erg s^{-1} (Böhringer et al. 2000). Böhringer et al. (2000) report a mass distribution elongated in the NNE–SSW direction (see also Dahle et al. 2002), but the available maps do not agree in detail. In fact, the primary peak of Holhjem et al. (2009) corresponds to the secondary one of Dahle et al. (2002) (cf. figure 3 – top-left panel – of Holjem et al. with figure 17 – top-right panel – of Dahle et al.). The *ROSAT* HRI image also reveals a clear elongation, roughly in the north–south direction (Giacintucci et al. 2009; Giovannini et al. 2009), thus suggesting ongoing merger activity (Allen et al. 2003).

As for the radio emission, Owen et al. (1999) reported the first evidence of a diffuse, extended source in this cluster. The analysis of VLA data archive at 1.4 GHz shows the presence of a centrally located, Mpc-extended source classified as a giant radio halo with a power $P_{1.4\rm GHz} = 1.2\text{-}{-}1.3 \times 10^{25}\ h_{70}^{-2}$ W Hz^{-1} (Giacintucci et al. 2009; Giovannini et al. 2009). Despite the particular difficulty of the subtraction of discrete sources present in radio maps, both analyses of Giacintucci et al. (2009) and Giovannini et al. (2009) show that the radio diffuse emission is quite asymmetric with respect to the X-ray peak. In particular, Giacintucci et al. suggest that the ridge in the southern peripheral region of the halo is a relic projected on to the radio halo emission (see their figure 2 and our Figure 1). A1351 is also an atypical cluster for its very large velocity dispersion of $\sigma_v = 1680^{+340}_{-230}$ km s^{-1}. This value and the published cluster redshift ($z = 0.3279$) are based on 17 cluster members (Irgens et al. 2002).

We acquired new spectroscopic and photometric data on the 3.5 m Telescopio Nazionale Galileo (TNG) and the 2.5 m Isaac Newton Telescope (INT), respectively. The present work is mainly based on these optical data. We also used optical data from the Sloan Digital Sky Survey, Data Release 7 (hereafter SDSS-DR7). We also use X-ray data from *Chandra* and *XMM-Newton* public archive to study the intracluster medium of A1351 and analyse its global morphological and spectral properties.

This paper is organized as follows. We present optical data and the cluster catalogue in Section 2. Our results on the cluster structure based on optical and X-ray analyses are presented in Sects 3 and 4, respectively. We discuss the cluster structure in Sect. 5 and present our conclusions in Section 6. Unless otherwise stated, we indicate errors at the 68% confidence level (hereafter c.l.). Throughout this paper, we use $H_0 = 70$ km s^{-1} Mpc^{-1} and $h_{70} = H_0/(70$ km s^{-1} Mpc$^{-1})$ in a flat cosmology with $\Omega_0 = 0.3$ and $\Omega_\Lambda = 0.7$. In the adopted cosmology, $1'$ corresponds to $\sim$282 h_{70}^{-1} kpc at the cluster redshift.

2 OPTICAL OBSERVATIONS

Multi-object spectroscopic (MOS) observations of A1351 were carried out at the TNG on 2010 March 10. We used DOLORES/MOS with the LR-B Grism 1, yielding a dispersion of 187 Å/mm. We used the 2048×2048 pixel E2V CCD, with a pixel size of 13.5 μm. In total, we observed four MOS masks including 143 slits. For each mask, the exposure time was 3×1800 s.

Reduction of spectra and radial velocity computation were performed using standard IRAF[2] tasks and the cross-correlation technique developed by Tonry & Davis (1979), as done with other clusters included in our DARC sample (for a detailed description see, for example, Boschin et al. 2012). Our spectroscopic catalogue lists 129 galaxies in the field of A1351 (see Table 1).

Comparing the velocity measurements for ten galaxies

[1] See also http://wwwuser.oats.inaf.it/girardi/darc/, the web site of the DARC project.

[2] IRAF is distributed by the National Optical Astronomy Observatories, which are operated by the Association of Universities for Research in Astronomy, Inc., under cooperative agreement with the National Science Foundation.

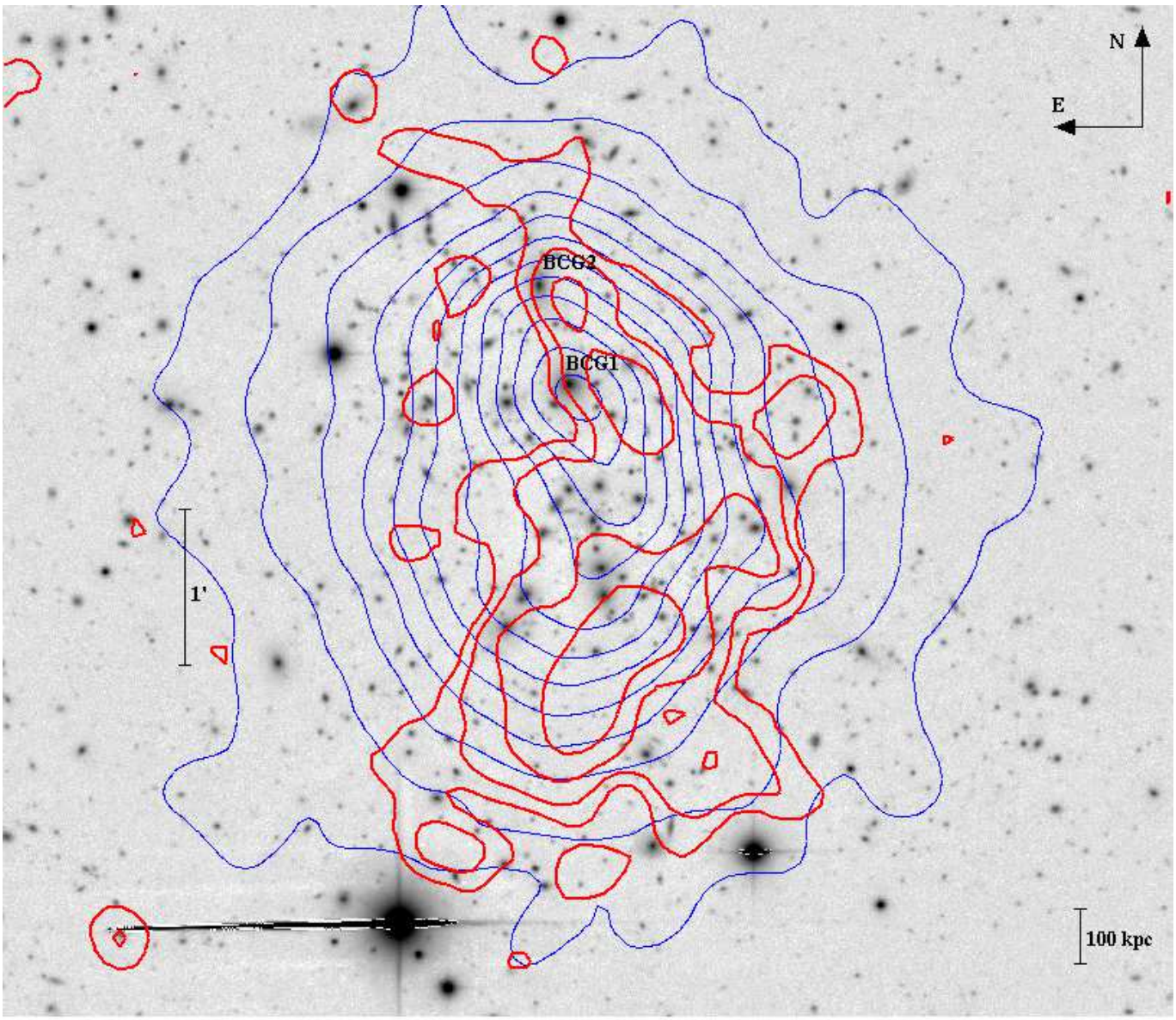

Figure 1. INT R-band image of the cluster A1351 (north at the top and east to the left) with, superimposed, the contour levels of the *Chandra* archival image ID 15136 (blue thin contours; photons in the energy range 0.3–7 keV) and the contour levels of a VLA radio image at 1.4 GHz (red thick contours, see Giacintucci et al. 2009). Labels highlight the positions of the two brightest cluster galaxies.

observed with multiple masks, we corrected the velocity errors provided by the cross-correlation technique by multiplying them for a factor 2.2 (see discussion in, e.g., Girardi et al. 2011, Boschin et al. 2004). Taking into account the above correction, the median value of the cz errors is 77 km s^{-1}. Three galaxies have spectroscopic redshift in SDSS-DR7 in good agreement with our values. We used magnitudes corrected for galactic extinction, *dereddened*, in the r', i', and g' photometric bands.

Table 1 lists the velocity catalogue (see also Fig. 2): identification number of each galaxy, ID (col. 1); right ascension and declination, α and δ (J2000, col. 2); r' magnitude from SDSS-DR7 (col. 3); heliocentric radial velocities, $v = cz_{\odot}$ (col. 4) with errors, Δv (col. 5).

We had already observed A1351 field with the Wide Field Camera (WFC), mounted at the prime focus of the 2.5 m INT telescope. We took exposures of 9×600 s and 9×300 s in B and R Harris filters in photometric conditions and $1.2''$ seeing. However, we used SDSS-DR7 data because a greater number of photometric bands are available, which allows an accurate colour analysis. INT and SDSS-DR7 photometric data are very similar. The completeness magnitude is $r' = 20.8$.

The position of the brightest cluster member galaxy (ID. 66 with $r' = 17.01$, hereafter BCG1) is very close to the peak of the X-ray emission and the peak of the mass distribution provided by Dahle et al. (2002). The second-brightest galaxy is ID. 66 with $r' = 17.73$ (hereafter BCG2), and then there are several other galaxies at similar brightness ($\Delta r' < 0.5$).

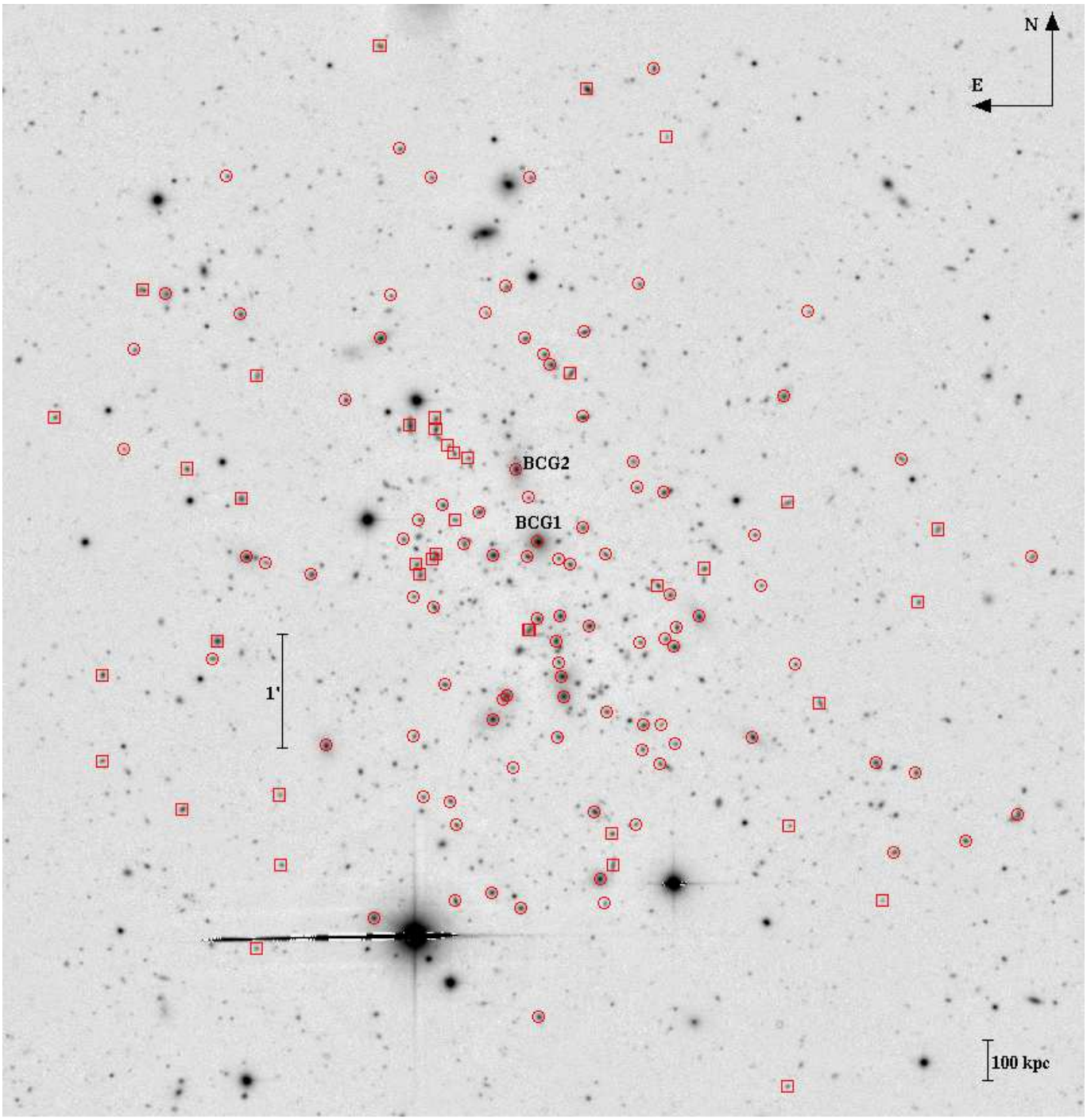

Figure 2. Galaxy sample observed spectroscopically, overlapping the INT *R*-band image of the cluster A1351. Circles and squares indicate cluster members and non-members, respectively (see Table 1). Labels indicate the brightest galaxy members.

3 ANALYSIS OF THE OPTICAL DATA

3.1 Cluster member selection

To select cluster members among the 129 galaxies with redshifts we performed the 1D adaptive-kernel method (hereafter 1D-DEDICA, Pisani 1993 and Pisani 1996; see also Fadda et al. 1996; Girardi et al. 1996). This procedure detected A1351 as a quite asymmetric peak at $z \sim 0.324$ populated by 100 galaxies. The re-running of the procedure rejected another two galaxies considered as 'isolated', leading to 98 galaxies and then to the detection of two peaks (see Figure 3). The second step in the member selection (which uses the combination of position and velocity information, i.e. the 'shifting gapper' method of Fadda et al. (1996; see also, e.g. Girardi et al. 2011 for details on the application of this technique) rejects three galaxies from the whole complex. We adopted as centre position the coordinates of the brightest cluster galaxy – BCG1 [R.A. = $11^{\rm h}42^{\rm m}24\overset{\rm s}{.}78$, Dec.

Table 1. Radial Velocities of 135 galaxies in the field of A1351. IDs in boldface highlight the two brightest cluster members BCG1 (ID. 66) and BCG2 (ID 74; see text). IDs in italics refer to non-member galaxies.

ID	α, δ (J2000)	r'	v (km	Δv s^{-1})
1	11 41 51.74, +58 31 56.4	20.36	96298	86
2	11 41 52.65, +58 29 41.4	19.10	95376	77
3	11 41 56.16, +58 29 27.7	19.78	96378	53
4	11 41 58.06, +58 32 11.0	20.11	131414	101
5	11 41 59.35, +58 31 33.0	20.61	117212	79
6	11 41 59.49, +58 30 03.6	19.85	99815	90
7	11 42 00.51, +58 32 48.1	20.14	98618	123
8	11 42 00.94, +58 29 21.8	19.69	96522	66
9	11 42 01.74, +58 28 57.0	21.58	223024	220
10	11 42 02.17, +58 30 09.0	19.26	97493	48
11	11 42 05.93, +58 30 40.2	20.10	18684	158
12	11 42 06.73, +58 34 05.6	21.03	97644	119
13	11 42 07.57, +58 31 00.6	20.76	97757	59
14	11 42 07.93, +58 29 36.0	21.79	404991	500
15	11 42 08.05, +58 27 19.5	21.19	126950	62
16	11 42 08.08, +58 32 25.4	20.07	60602	81
17	11 42 08.39, +58 33 21.2	18.66	99683	75
18	11 42 09.88, +58 31 42.1	21.18	99562	95
19	11 42 10.29, +58 32 08.6	20.77	97823	79
20	11 42 10.41, +58 30 22.5	18.89	95304	39
21	11 42 13.67, +58 31 50.9	20.14	116817	114
22	11 42 13.99, +58 31 25.9	18.59	98855	37
23	11 42 15.51, +58 31 20.3	19.82	94808	70
24	11 42 15.57, +58 30 19.0	20.65	94702	88
25	11 42 15.64, +58 31 09.9	18.85	99819	84
26	11 42 15.96, +58 31 37.1	19.88	95611	70
27	11 42 16.24, +58 31 14.1	20.41	96996	81
28	11 42 16.28, +58 35 37.0	21.59	19432	156
29	11 42 16.39, +58 32 30.9	19.79	101230	70
30	11 42 16.52, +58 30 29.3	21.43	95433	110
31	11 42 16.59, +58 30 08.8	20.70	96742	86
32	11 42 16.77, +58 31 42.3	19.99	86266	68
33	11 42 17.13, +58 36 13.2	19.83	98554	66
34	11 42 17.68, +58 30 28.9	19.44	99607	57
35	11 42 17.77, +58 30 16.2	20.33	94769	81
36	11 42 17.93, +58 31 12.5	20.61	99725	114
37	11 42 18.07, +58 34 20.2	20.66	99856	77
38	11 42 18.18, +58 32 33.5	20.63	99328	73
39	11 42 18.19, +58 29 36.9	21.14	96715	101
40	11 42 18.42, +58 32 47.1	20.47	97793	147
41	11 42 19.73, +58 29 15.6	19.73	71610	130
42	11 42 19.77, +58 29 32.2	20.31	126880	110
43	11 42 20.17, +58 30 36.0	20.08	97199	70
44	11 42 20.25, +58 28 55.6	21.19	95157	127
45	11 42 20.29, +58 31 58.6	20.13	95813	81
46	11 42 20.58, +58 29 08.4	18.15	96208	132
47	11 42 20.93, +58 29 43.5	19.00	97843	64
48	11 42 21.35, +58 31 21.2	19.09	96142	48
49	11 42 21.57, +58 36 02.2	18.85	60383	62
50	11 42 21.73, +58 33 55.4	19.56	96492	45
51	11 42 21.79, +58 32 12.7	19.57	97021	68
52	11 42 21.80, +58 33 10.6	19.08	99953	64
53	11 42 22.64, +58 33 33.6	19.54	46718	86
54	11 42 22.66, +58 31 53.4	19.96	97289	51
55	11 42 23.03, +58 30 44.2	18.17	97054	55
56	11 42 23.16, +58 30 54.6	18.18	98169	53
57	11 42 23.27, +58 31 26.2	19.00	96208	88
58	11 42 23.40, +58 30 22.8	19.86	98791	90
59	11 42 23.40, +58 31 02.1	20.60	98118	77
60	11 42 23.40, +58 31 56.4	20.66	96609	92
61	11 42 23.57, +58 31 13.1	19.50	94118	66
62	11 42 23.97, +58 33 38.0	19.10	96433	64
63	11 42 24.39, +58 33 43.6	20.20	98597	66
64	11 42 24.62, +58 27 56.3	19.84	97922	54
65	11 42 24.77, +58 31 24.9	19.24	93425	53
66	11 42 24.78, +58 32 05.3	17.01	96531	28
67	11 42 25.34, +58 31 19.3	19.70	39316	101
68	11 42 25.37, +58 35 16.1	20.32	99142	117
69	11 42 25.38, +58 31 18.9	19.00	39337	79
70	11 42 25.44, +58 32 28.4	20.87	98894	84
71	11 42 25.50, +58 31 57.6	19.46	100922	171
72	11 42 25.68, +58 33 51.9	19.99	98377	86
73	11 42 25.87, +58 28 53.2	19.66	95012	68
74	11 42 26.25, +58 32 43.3	17.73	100224	55
75	11 42 26.42, +58 30 07.0	20.96	96765	101
76	11 42 26.83, +58 30 44.7	18.21	95862	53
77	11 42 26.96, +58 34 19.2	19.85	98930	81
78	11 42 27.09, +58 30 42.9	20.46	95532	88
79	11 42 27.78, +58 30 32.3	18.22	96321	32
80	11 42 27.80, +58 31 58.3	18.64	99455	30
81	11 42 27.82, +58 29 01.4	19.48	95521	70
82	11 42 28.29, +58 34 05.3	21.29	95519	119
83	11 42 28.73, +58 32 20.9	19.56	97331	77
84	11 42 29.46, +58 32 49.4	20.73	86542	77
85	11 42 29.72, +58 32 04.3	20.07	99727	84
86	11 42 30.20, +58 29 36.8	20.26	94471	59

$= +58^\circ 32' 05.3''$ (J2000.0)], which coincides with the location of the peak of the X-ray emission. However, note that A1351 is an elongated cluster with BCG1 lying in the northern region (see in the following). Summarizing, we analysed the structure of A1351 using 95 fiducial cluster members.

By applying the biweight estimator to the 95 cluster members (Beers et al. 1990, ROSTAT software), we computed a mean cluster redshift of $\langle z \rangle = 0.3247 \pm 0.0005$, i.e. $\langle v \rangle = (97\,350 \pm 157)$ km s^{-1}. We estimated the LOS velocity dispersion, σ_V, by using the biweight estimator and applying the cosmological and standard corrections for velocity errors (Danese et al. 1980), respectively. We obtained $\sigma_V = 1524^{+96}_{-74}$ km s^{-1}, where the errors are computed through a bootstrap technique. To verify the robustness of the σ_V estimate, we analysed the velocity dispersion profile, which is consistent with a flat shape (Fig. 4).

3.2 Substructure analysis

In the velocity distribution of the 95 member galaxies, the 1D-DEDICA procedure detects two significant peaks (DED1 and DED2) of 60 and 35 galaxies, at 96 525 and 99 134 km s^{-1}. These peaks largely overlap with 22 (of DED1) and 19 (of DED2) galaxies with a high probability of belonging to the other peak too, see Fig. 5. BCG1 and BCG2 belong to the DED1 and DED2 subclusters, respectively. Mean velocities and velocity dispersions, as computed on subclus-

Table 1. Continued.

ID	α, δ (J2000)	r'	v (km s^{-1})	Δv
87	11 42 30.21, +58 28 57.2	19.01	96268	53
88	11 42 30.35, +58 32 16.9	20.58	132539	84
89	11 42 30.42, +58 32 51.7	20.51	102690	68
90	11 42 30.58, +58 29 49.3	20.14	95192	64
91	11 42 30.81, +58 32 55.8	21.33	87000	220
92	11 42 31.00, +58 30 50.5	19.94	97625	42
93	11 42 31.14, +58 32 24.5	19.97	95732	53
94	11 42 31.61, +58 31 58.8	19.47	46323	66
95	11 42 31.65, +58 33 04.5	19.13	101910	64
96	11 42 31.66, +58 33 10.1	20.31	39311	75
97	11 42 31.71, +58 31 31.2	19.62	98490	73
98	11 42 31.80, +58 31 56.5	20.14	146049	81
99	11 42 32.00, +58 35 16.4	20.69	96579	106
100	11 42 32.40, +58 29 51.6	20.66	93838	99
101	11 42 32.67, +58 31 48.1	19.46	46519	79
102	11 42 32.73, +58 32 17.0	20.58	96760	77
103	11 42 32.90, +58 31 53.6	20.29	145458	86
104	11 42 33.02, +58 30 23.5	20.59	96943	64
105	11 42 33.11, +58 31 36.7	20.84	94982	86
106	11 42 33.37, +58 33 06.4	18.43	19387	55
107	11 42 33.77, +58 32 06.7	20.40	99125	88
108	11 42 34.12, +58 35 31.2	20.49	100946	73
109	11 42 34.69, +58 34 14.4	21.16	99974	101
110	11 42 35.38, +58 33 52.1	18.41	99892	35
111	11 42 35.46, +58 36 25.1	19.80	18306	198
112	11 42 35.66, +58 28 48.1	19.56	100490	51
113	11 42 37.71, +58 33 19.8	19.91	96834	44
114	11 42 38.92, +58 30 18.8	18.37	93762	51
115	11 42 39.92, +58 31 48.6	19.65	100309	112
116	11 42 41.88, +58 29 16.3	20.68	143417	73
117	11 42 41.98, +58 29 52.9	20.65	143144	97
118	11 42 42.99, +58 31 54.6	20.82	93791	103
119	11 42 43.52, +58 28 32.4	20.99	173827	75
120	11 42 43.64, +58 33 32.3	20.24	112154	158
121	11 42 44.29, +58 31 57.7	18.38	95717	48
122	11 42 44.65, +58 32 28.3	19.59	19164	110
123	11 42 44.74, +58 34 04.8	19.62	96833	73
124	11 42 45.68, +58 35 17.0	20.86	99277	75
125	11 42 46.22, +58 31 13.4	18.98	103511	53
126	11 42 46.51, +58 31 04.3	20.44	93695	88
127	11 42 48.29, +58 32 43.8	19.96	19592	48
128	11 42 48.48, +58 29 45.4	19.71	110746	90
129	11 42 49.75, +58 34 15.6	19.29	98495	59
130	11 42 51.26, +58 34 17.3	19.61	19534	101
131	11 42 51.82, +58 33 46.3	20.68	99361	66
132	11 42 52.52, +58 32 54.3	20.90	99326	108
133	11 42 53.87, +58 30 10.7	20.56	124723	95
134	11 42 53.88, +58 30 55.8	19.94	74514	90
135	11 42 57.15, +58 33 10.9	20.52	130786	103

ter members, are $\langle v_{\rm DED1}\rangle = 96\,191$ km s^{-1} and $\langle v_{\rm DED2}\rangle = 99\,433$ km s^{-1}and $\sigma_{v,\rm DED1} = 940$ km s^{-1} and $\sigma_{v,\rm DED2} = 584$ km s^{-1}. The distributions of galaxy positions of DED1 and DED2 are different at the 99.4% c.l. according to the the 2D Kolmogorov–Smirnov test (Fasano & Franceschini 1987, hereafter 2D-KS), see Figure 7.

The 1D-Kaye mixture model test (1D-KMM; Ashman et al. 1994; see also Boschin et al. 2012, Boschin et al. 2013 for recent applications), finds a two-Gaussian partition which is a better descriptor than a one-Gaussian profile at the 98.4% and 96.5% c.l.s for the homoscedastic and heteroscedastic cases (i.e. the cases assuming equal or different dispersions), respectively. The Gaussians corresponding to the heteroscedastic case, which is the more realistic approach, are shown in Figure 5. The two subsamples detected by 1D-KMM contain 62 and 33 members (KMM1 and KMM2), where several galaxies have a high probability of belonging to both the peaks. For the two Gaussians we obtain mean velocities, $\langle v_{\rm KMM1}\rangle = 96\,328$ km s^{-1} and $\langle v_{\rm KMM2}\rangle = 99\,538$ km s^{-1}, and velocity dispersions, $\sigma_{v,\rm KMM1} = 1\,384$ km s^{-1} and $\sigma_{v,\rm KMM2} = 783$ km s^{-1}, where the galaxies are weighted according to their partial membership of both groups so as to avoid possible underestimates connected with an artificial truncation of the tails of the samples. The distributions of the galaxy positions of KMM1 and KMM2 are different at the 99.3% c.l. according to the the 2D-KS.

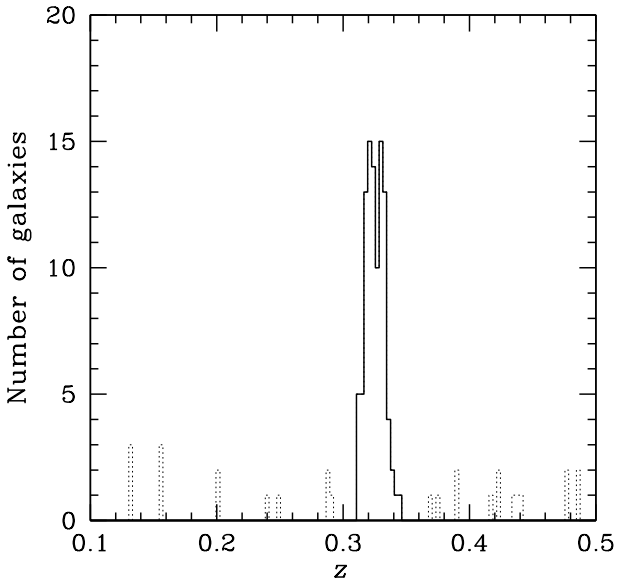

Figure 3. Redshift galaxy distribution. The solid line histogram refers to the 100 galaxies assigned to A1351 according to the 1D-DEDICA reconstruction method.

Concerning the spatial distribution of galaxies in the plane of the sky, we analysed the photometric SDSS catalogues extracted for a 30′radius region from the cluster centre thus to overcome redshift and spatial incompleteness of our spectroscopic catalogue. We performed a member selection based on both (r'–i' vs. r') and (g'–r' vs. r') colour–magnitude relations following, for example, the Boschin et al. (2012) prescriptions; here r'–i'=0.956-0.019r' and g'–r'=2.841-0.244r'. The 2D-DEDICA analysis detects A1351 as only one isolated peak in the space of projected positions (see Figure 6).

We also applied a set of 3D tests combining velocity and position information. We applied the Δ-statistics devised by Dressler & Schectman (1988, hereafter DS-test), also with the alternative kinematic estimators separating mean velocity and velocity dispersion (hereafter DS$\langle v\rangle$-test and DSσ_v-test, e.g. Ferrari et al. 2003; Girardi et al. 2010,

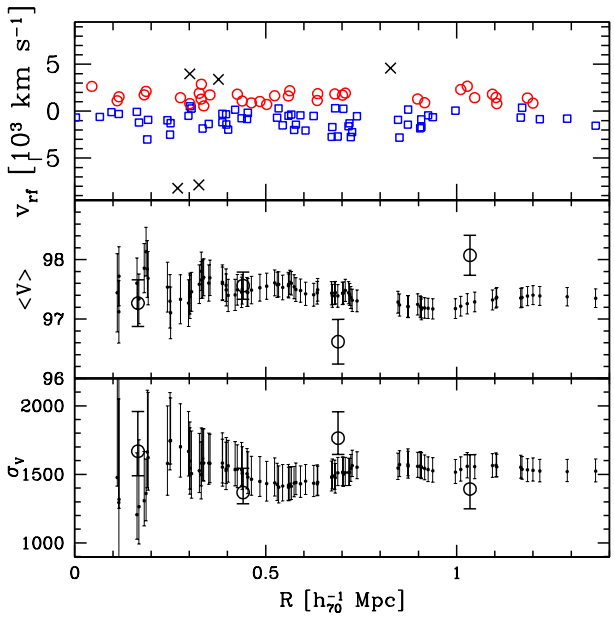

Figure 4. *Top panel:* rest-frame velocity vs. projected cluster-centric distance for the 100 member galaxies belonging to the peak in the velocity distribution (Fig. 3). Crosses indicate galaxies rejected as interlopers by the 'shifting gapper' procedure. Blue squares and red circles indicate the 95 member galaxies as divided in the DED1 and DED2 subsamples. The cluster centre coincides with the position of the BCG1. *Middle and bottom panels:* differential (big circles) and integral (small points) profiles of mean velocity and LOS velocity dispersion, respectively. For the differential profiles, we plot the values for four annuli from the centre of the cluster, each of 0.3 h_{70}^{-1} Mpc. For the integral profiles, the mean and dispersion at a given (projected) radius from the cluster centre is estimated by considering all galaxies within that radius – the first value computed on the five galaxies closest to the centre. The error bands at the 68% c.l. are also shown.

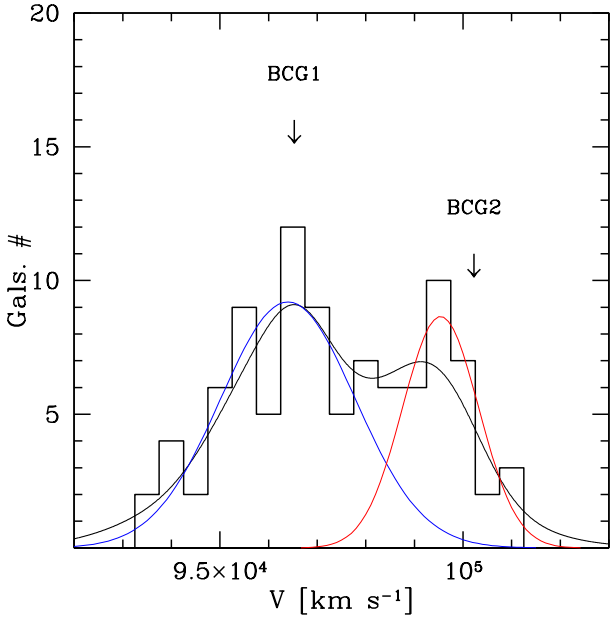

Figure 5. Velocity distribution of the 95 galaxies assigned to the cluster. The arrows indicate the velocity of the BCG1 and BCG2. Black curve is the density reconstruction according to the 1D-DEDICA method. Red and blue Gaussian profiles are the best bimodal fits according to the 1D-KMM test.

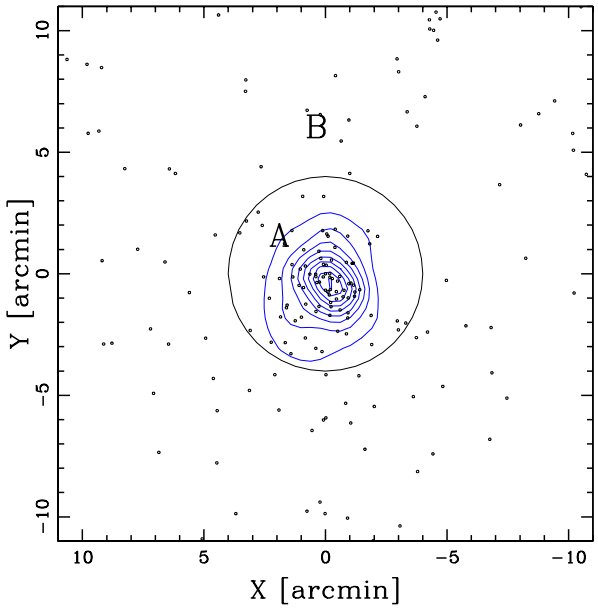

Figure 6. A large scale spatial distribution on the sky and relative isodensity contour map of likely cluster members extracted from the SDSS photometric catalogue with $r' \leqslant 21.5$. The contour map is obtained with the 2D-DEDICA method (blue lines). The $4'$ circle outlines the region sampled by our spectroscopic data. The two labels indicate the two secondary peaks in the mass distribution according to the weak lensing analysis by Holhjem et al. (2009).

1997). We applied the ϵ-test (Bird & Beers 1993) based on the projected mass estimator and the centroid shift or α-test (West & Bothun 1990). The presence of a velocity gradient was analysed performing a multiple linear regression fit to the observed velocities with respect to the galaxy positions in the plane of the sky (e.g. den Hartog & Katgert 1996). The significance of the results is based on 1000 Monte Carlo simulated clusters where original position and velocities are shuffled. We found that substructure is significant in the case of the the ϵ-test, which is sensitive to the combined values of local velocity dispersion and projected density at the $> 99.9\%$ c.l. The DS-test detects substructure significant at the 98.8% c.l., in practice owing to the mean velocity estimator (for DS$\langle v \rangle$-test the significance is at the 99.7% c.l.). We also found a $> 99.9\%$ c.l. significant velocity gradient with a position angle $PA = -16^{+14}_{-18}$ degrees (measured counter-clockwise from the north), i.e. higher-velocity galaxies lie in the north (see Figure 7). Figure 7 shows that galaxies in the external cluster region are responsible for the position–velocity correlation.

We also resorted to the Htree-method devised by Serna & Gerbal (1996); a similar technique is also used to determine cluster members (Serra & Diaferio 2013). The method uses a hierarchical clustering analysis to determine

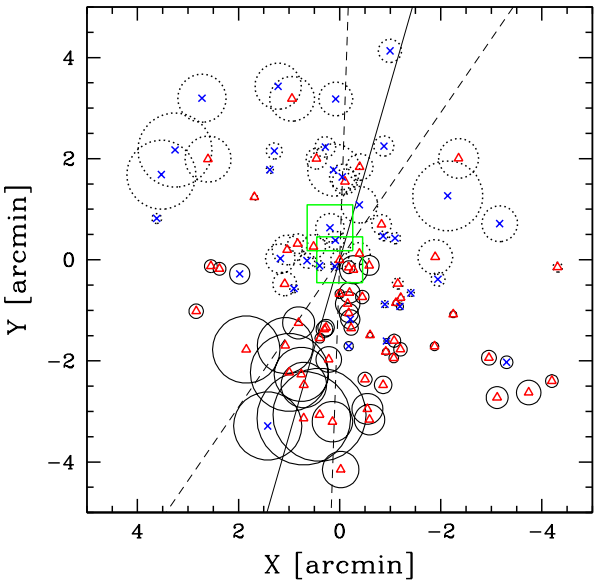

Figure 7. Spatial distribution of the 95 cluster members, where small blue triangles and red crosses indicate the DED1 and DED2 members. Each galaxy is marked by a circle: the larger the circle, the larger is the deviation of the local mean velocity from the global mean velocity. Thin/solid and thick/dotted circles show where the local value is smaller or larger than the global value. The plot is centred on the cluster centre (=BCG1). BCG1 and BCG2 are indicated by faint large/green squares. The solid and dashed lines indicate the position angle of the cluster velocity gradient and relative errors, respectively.

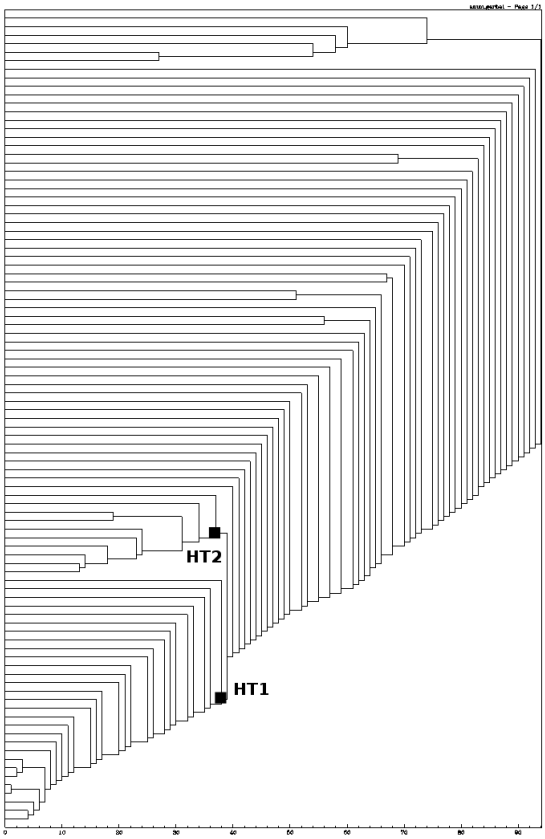

Figure 8. Dendogram obtained through the Serna & Gerbal (1996) algorithm (here M/L_r=150 h_{70} $M_\odot/L_\odot$). The abscissa is the binding energy (here in arbitrary unit with the deepest negative energy levels on the left). The two main subclusters are indicated by HT1 and HT2.

the relationship between galaxies according to their relative binding energies where ignorance of the mass associated with each galaxy is overcome adopting for each galaxy halo the typical mass-to-light of galaxy cluster. The clustering sequence can be visualized in the form of a hierarchical tree diagram (dendogram). Figure 8 shows the resulting dendogram, where we used M/L_r=150 h_{70} $M_\odot/L_\odot$, as suggested by broad statistical studies (e.g. Girardi et al. 2000; Popesso et al. 2005). From Fig. **??** it can be seen that A1351 contains two main subgroups (HT1 and HT2), with BCG1 and BCG2 in the respective potential well. The presence of the two subgroups is quite robust against the choice of the value of M/L_r, although the number of identified members depends on the precise value of M/L_r, i.e. it decreases with the increase in M/L_r from 100 to 200 h_{70} $M_\odot/L_\odot$. HT1 and HT2 are well separated in velocity and superimposed in the sky in the central cluster region (see Fig. 9 and insert plot). Their mean velocities are $\langle v_{\rm HT1}\rangle = 96\,540$ km s^{-1} and $\langle v_{\rm KMM2}\rangle = 99\,697$ km s^{-1}. Our interpretation is that they are the central, densest parts of the two subclusters detected through the KMM or the 1D-DEDICA method (see above).

4 X-RAY MORPHOLOGICAL AND SPECTRAL ANALYSIS

In order to complement our optical analysis, we used recent X-ray data taken with *Chandra* and *XMM-Newton* satellites to study the ICM of A1351 and infer its global morphological and spectral properties.

First, we considered archival data taken with the *Chandra* Advanced CCD Imaging Spectrometer (ACIS–I; exposure ID 15136). We reduced the data using the CIAO package[3] (version 4.2) on chips I0, I1, I2 and I3 (total field of view $\sim 17' \times 17'$) in a standard way (see Boschin et al. 2004)

A quick look at the reduced image suggests the ICM is somewhat elongated in the NNE–SSW direction (see Figure 10). A clear twisting of the isophotes is present (see Fig. 1), from the centre towards the more external regions, thus suggesting the ICM is not relaxed in a regular gravitational potential well.

To better characterize the X-ray morphology of the cluster we performed a wavelet multiscale analysis on chip I3 with the CIAO/WAVDETECT task. On small scales (2–6 pixels), taking advantage of the high spatial resolution of *Chandra* images, WAVDETECT was effective in identifying the pointlike sources projected on the line of sight of the cluster. After removal of these sources, a run of WAVDETECT on larger scales (20–42 pixels) allowed us to identify four X-ray clumps (see Fig. 11), thus confirming the irregular morphology of the ICM.

[3] see http://asc.harvard.edu/ciao/

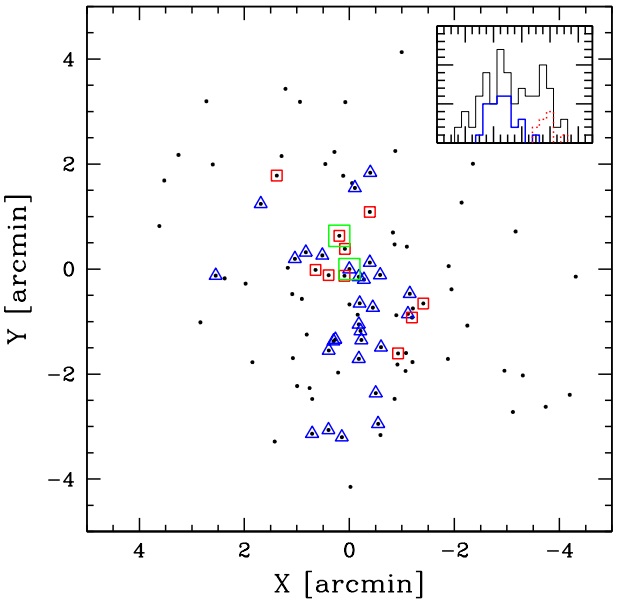

Figure 9. Spatial distribution on the sky of 95 cluster members (black points). Blue triangles and red squares indicate galaxies of HT1, the main subcluster, and HT2, the secondary subcluster. BCG1 and BCG2 are highlighted by large, green squares. The insert plot shows the same velocity distribution of subcluster galaxies (blue/solid dotted and red/dotted lines for HT2 and HT1).

These clumps are also evident when fitting a simple β-model profile to the 2D X-ray photon distribution and analysing the model residuals. The model is defined to be (Cavaliere & Fusco-Femiano 1976):

$$S(\mathrm{R}) = S_0[1 + (\mathrm{R}/\mathrm{R_c})^2]^{\alpha} + b, \quad (1)$$

where R is the projected radial coordinate from the centroid position and b the surface brightness background level. The fit only provides poorly constrained and unrealistic values of the slope parameter α and the angular core radius $\mathrm{R_c}$ ($\alpha = -4.4^{+0.5}_{-0.4}$, $\mathrm{R_c} = 163.1'' \ ^{+12.6''}_{-10.7''} = 766.6^{+59.2}_{-50.2}\ h_{70}^{-1}$ kpc at the cluster redshift), which is another hint of an irregular X-ray photon distribution. Moreover, the analysis of the β-model residuals reveals a clear excess of X-ray emitting gas in correspondence with the four clumps detected by the wavelet multiscale analysis (see Figure 11).

As for the spectral properties of the cluster X-ray photon distribution, we computed global ICM temperature by analysing *XMM-Newton* data. We considered an observation of A1351 (ID 0650382201) stored in the public archive. We reprocessed the Observation Data Files (ODF) using the Science Analysis System (SAS; version 13.0), following the procedure described in De Grandi & Molendi (2009) to produce calibrated event list cleaned of soft protons. The net exposure time of the observation is 5.2 ks for MOS1, 6.7 ks for MOS2 and 2.5 ks for the *pn*.

We applied the background subtraction using blank-sky fields for EPIC MOS and *pn* produced by Leccardi & Molendi (2008). Using the XSPEC package (version 11.3.2, Arnaud 1996), we analysed the EPIC spectrum of an elliptical region centred on coordinates $\alpha =$ 11:42:24.28 and $\delta = +$58:31:30.94, with $a = 2.5'$, a/b=1.25 (where a and b are the major and minor axes, respectively) and PA=15°(measured from north to east; see Figure 12). We modelled the spectrum with a one-temperature thermal model with the plasma in collisional ionization equilibrium (*apec* model in XSPEC), multiplied by a *wabs* absorption model with the Galactic hydrogen column density fixed at $N_{\mathrm{H}} = 9.94 \times 10^{19}$ cm^{-2} (Kalberla et al. 2005). We found that the ICM has a global temperature of $kT = 8.62^{+0.96}_{-0.61}$ keV.

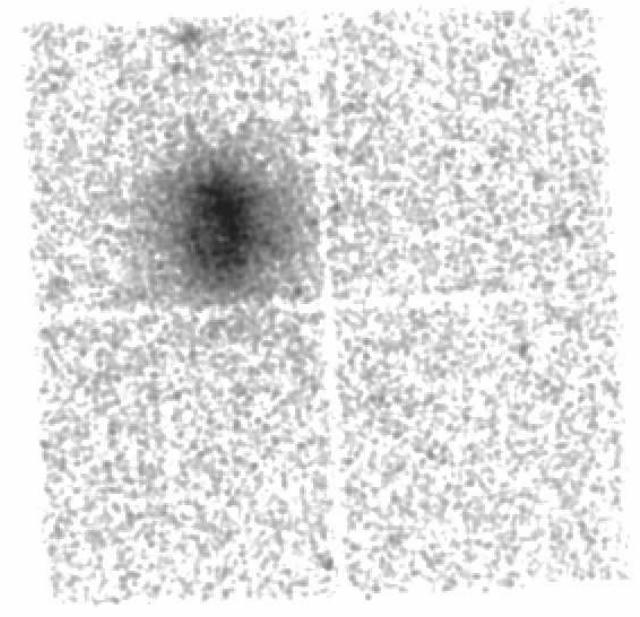

Figure 10. $17' \times 17'$ *Chandra* ACIS-I X-ray image (ID 15136) of A1351 in the energy band 0.3–7 keV (north at the top and east to the left; binned by 8×8 pixels and Gaussian-smoothed with σ=2 pixels).

5 CLUSTER STRUCTURE

We present several proofs in favour of the previous first evidence of an ongoing merger activity in A1351. Our kinematic analysis is based on a factor $>$ 5 more galaxies than previously. On the one hand, we confirm that A1351 is characterized by a high global value of velocity dispersion $\sigma_{\mathrm{V}} = 1524^{+96}_{-74}$ km s^{-1} (see $\sigma_v = 1680^{+340}_{-230}$ km s^{-1}, Irgens et al. 2002) and, on the other hand, it shows a bimodal velocity distribution with two peaks separated by $\sim$2500 km s^{-1} in the rest frame. As for the X-ray data, we confirm the N–S elongation of the X-ray emission and further features are detected. From north to south we detected three, maybe four, substructures (see Figure 11). The northern part, containing the two most important X-ray clumps, is particularly brighter and is NNE–SSW elongated. BCG2 and BCG1 bright galaxies are placed along the N–S direction. In addition, a few other quite luminous members (IDs. 55, 56, 76, 79) are aligned following the same axis. Moreover, we detected a velocity gradient in the galaxy velocity field roughly in S–N direction and the presence of 3D substructure at a very significant level.

The above results indicate that the cluster structure

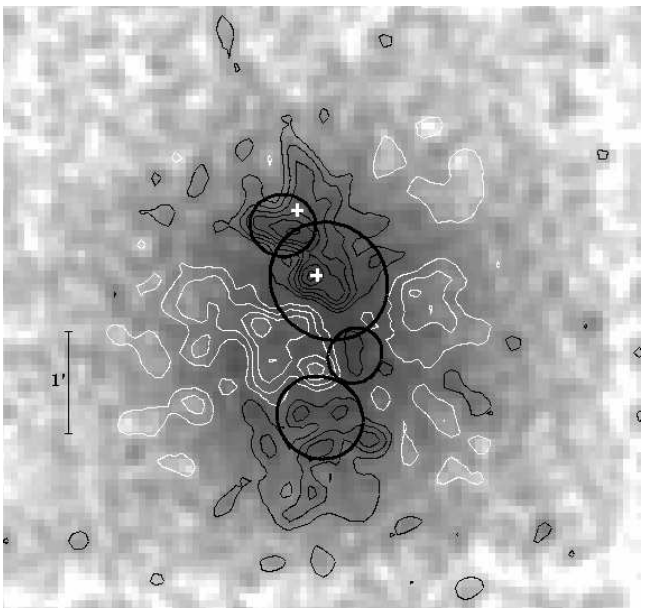

Figure 11. The smoothed X-ray emission in the left-upper quadrant of Fig. 10 with, superimposed, the contour levels of the positive (black thin contours) and negative (white thin contours) smoothed β-model residuals (north at the top and east to the left). Thick ellipses represent the X-ray clumps found by the wavelet multiscale analysis. As a reference, crosses highlight the positions of BCG1 and BCG2.

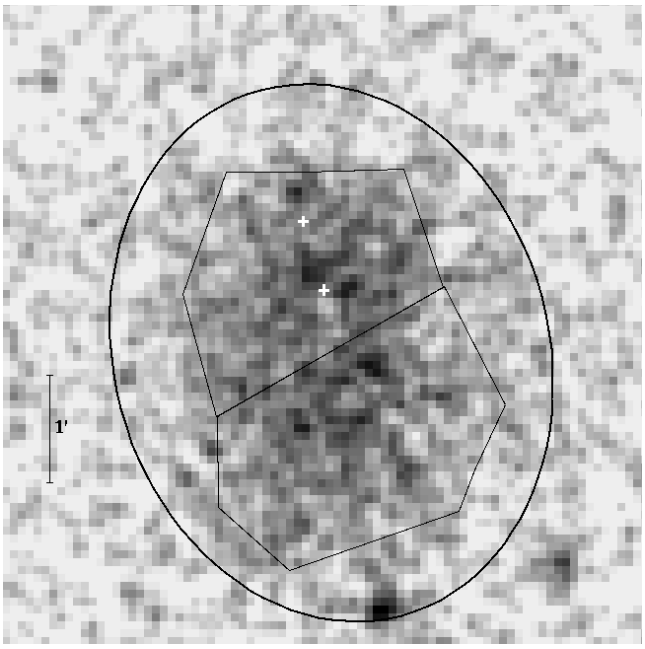

Figure 12. *XMM* smoothed image (ID 0650382201) of A1351 in the energy band 2–10 keV (north at the top and east to the left). Ellipse and polygons define the regions considered for the measurement of the ICM temperatures. As a reference, crosses show the positions of BCG1 and BCG2.

extends along the LOS but is not completely aligned with it. In particular, the two main subclusters, corresponding to BCG1 and BCG2 and detected as two northern X-ray clumps, cause the bimodality of the velocity distribution, low and high velocity peaks respectively (see Fig. 5). In spite of the very significant 3D substructure tests, we cannot detect two separate galaxy concentrations. This is probably because the two subclusters are so closely projected on the sky that we would need a much larger number of redshifts to sample the region better. The southern region, mostly populated by galaxies of the low velocity peak, is instead characterized by two less important substructures that contribute to trace the north–south direction.

The high value of the X-ray temperature, $kT = 8.69^{+1.01}_{-0.54}$ keV, indicates a high mass value, e.g. $M_{500} \sim 1.1 \times 10^{15}\ h_{70}^{-1}\ M_{\odot}$ and $M_{200} \sim 1.8 \times 10^{15}\ h_{70}^{-1}\ M_{\odot}$ (Lopeset al. 2009), as obtained from two published M–T relations. Alternatively, we used a kinematic approach, taking advantage of our redshift sample. We followed the prescriptions of Girardi & Mezzetti (2001, see also Girardi et al. 1998) by considering that A1351 is probably formed by two subclusters: the low velocity one, with $\sigma_{v,1}$ = 900-1400 km s^{-1}, and the high-velocity one, with $\sigma_{v,2}$ = 600-800 km s^{-1}. We obtained $M_1(< R_{200,1} = 1.9 - 2.8\ h_{70}^{-1}\mathrm{Mpc}) = 1.1 - 3.6 \times 10^{15}\ h_{70}^{-1}\ M_{\odot}$ and $M_2(< R_{200,2} = 1.2 - 1.6\ h_{70}^{-1}\mathrm{Mpc}) = 0.3 - 0.6 \times 10^{15}\ h_{70}^{-1}\ M_{\odot}$, and a global value of $M_{\rm sys}$ = 1.4-4.2 $\times 10^{15}\ h_{70}^{-1}\ M_{\odot}$. A1351 is thus quite a massive system, in agreement with typical mass values of other clusters hosting radio haloes (e.g. Girardi et al. 2008; Girardi et al. 2010) and in line with the expectations of the re-acceleration scenario in favouring more massive systems (e.g. Cassano et al. 2008).

The value of the velocity dispersion of the main subcluster, $\sigma_{v,1}$ = 900-1400 km s^{-1}, is consistent with the $\sigma_{\rm v,SIS}$ value of the singular isothermal sphere in the weak gravitational analysis ($\sigma_{v,1}$ = 1000-1400 km s^{-1}, Dahle et al. 2002; Holjem et al. 2009). The lower limit of our mass estimate, $M_{\rm sys}$ = 1.4–4.2 $\times 10^{15}\ h_{70}^{-1}\ M_{\odot}$, is only slightly above the lensing mass of Holjem et al. (2009), M_{200} = 8-9 $\times 10^{14}\ h_{70}^{-1}\ M_{\odot}$, when taking into account their smaller estimate of the value of R_{200} (1.69 h_{70}^{-1} Mpc, see our above estimate of $R_{200,1}$). Instead, we disagree with the morphological details of the two previous gravitational lensing analyses of Dahle et al. (2002) and Holhjem et al. (2009), which, in fact, are in disagreement with each other (see Section 1). In particular, as for the northern minor peak 'B' detected by Holhjem et al. (2009), this is outside the field we sampled through TNG redshift data and it is not detected by our analysis of the SDSS photometric sample (see Fig. 6), where the presence of A1351 is outstanding. Indeed, Holhjem et al. (2009) have suggested the possibility that peak 'B' is only a chance alignment of galaxies. The important LOS elongation of the structure of A1351 might be the cause the difficulties in the weak gravitational lensing analysis, in particular in determining the concentration parameter (Holhjem et al. 2009).

The elongation and twisting of isophotes of the X-ray emission is strong evidence for an ongoing cluster merger. With the available *XMM-Newton* observation we did not find any X-ray temperature difference between northern and southern regions (see Figure 12).

Reducing the complex structure of A1351 to the two

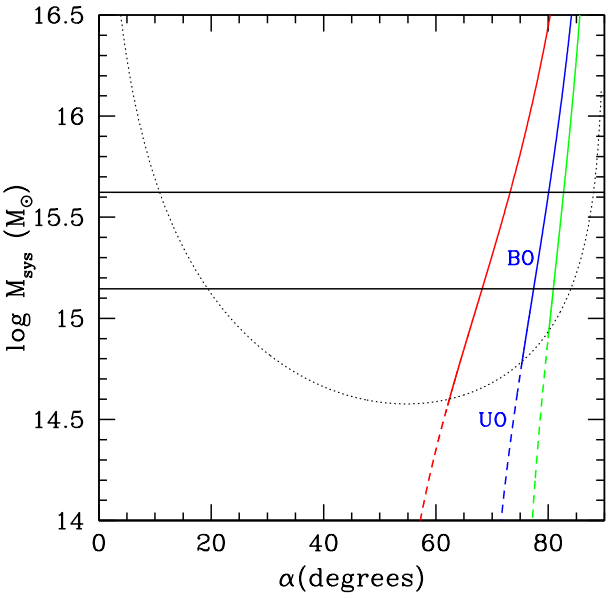

Figure 13. System mass vs. projection angle diagram of the two-body model applied to the two (main) subclusters. Solid and dashed lines correspond to bound bf (BO) and unbound (UO) outgoing solutions, respectively, where the elapsed time from the core crossing is $t = 0.1$, 0.2 and 0.3 Gy (from left to right, i.e. red, blue and green lines). The total mass of the system is represented by the horizontal line. The Newtonian criterion separates bound and unbound regions, above and below the thin dotted curve, respectively.

main subclusters, we can apply a model to follow the merging kinematics. We applied the analytic method of the bimodal model (Beers et al. 1982; Thompson 1982; see also Girardi et al. 2008 for a recent application). As for the input values of the relevant parameters for this model, we used the above $M_{\rm sys} = 1.4\text{-}4.2 \times 10^{15}\ h_{70}^{-1}\ M_\odot$ and the rest-frame LOS velocity difference between the two subclusters that measured $\Delta V_{\rm rf,LOS} \sim 2500$ km s^{-1}in both the DEDICA and KMM analyses . As for the projected distance between the two subclusters, our substructure analysis suggests a small value and does not allow a precise estimate. We then resorted to that measured between BCG1 and BCG2, $D \sim 0.2\ h_{70}^{-1}$ Mpc. In other clusters hosting radio haloes the time, t, elapsed from the core crossing is $t = 0.1$–0.3 Gyr (e.g. Markevitch et al. 2002; Girardi et al. 2008). For the cases with $t = 0.1$, 0.2 and 0.3 Gy, Figure 13 shows the outgoing solutions of the bimodal model as a function of α, the projection angle between the plane of the sky and the line connecting the centres of the two clumps, with the observed mass of the system $M_{\rm sys}$. The post core-crossing scenario represented by the bound outgoing solutions (BO) leads to a range of $\alpha \gtrsim 65$–$80°$. This value agrees with observational evidence of two main subclusters aligned mostly, but not completely, along the LOS.

Regarding the diffuse radio emission and its peculiar asymmetry with respect to the X-ray peak, Giacintucci et al. (2009) have suggested that the southern X-ray emission, the 'ridge', might be a relic rather a southern extension of the radio halo. Our results strongly support the above hypothesis. In fact, the northern part of the radio emission coincides with the region where the two main subclusters are projected. Consequently, the northern part of the radio emission can be correctly interpreted as a radio halo centrally located and someway symmetric with respect to the X-ray central emission, in agreement with typical radio halos in clusters. Excluding the contribution of the ridge, A1351 is much closer to the relation between the radio power and X-ray luminosity, as traced by the clusters showing a giant radio halo, as is shown well in fig. 3 of Giacintucci et al. (2009). The southern part of the radio emission (the ridge) lies at the external border of the most southern X-ray clumps. Thus, it could most probably be a relic connected to a merger along the north–south direction involving minor galaxy clumps. The only (minor) point of their scenario we cannot agree with is the northern small radio filament (see their figure 2). In this respect, we found no extension in the X-ray emission and no evidence of an optical subcluster in that region.

6 SUMMARY AND CONCLUSIONS

Our analysis of A1351 at $z \sim 0.3$, based on new spectra acquired at the TNG for ∼100 member galaxies, and X-ray data retrieved from *Chandra* and *XMM* archives, derives the following results:

- the measured dispersion of galaxy velocities is so high, $\sigma_{\rm V} \sim 1500$ km s^{-1}, owing to the bimodal structure of the velocity distribution;
- the measured X-ray temperature, $kT \sim 9$ keV, is also high, and both X-ray and kinematic data lead to a high mass value ($1\text{–}4 \times 10^{15}\ h_{70}^{-1}\ M_\odot$), in agreement with observational estimates of most clusters hosting radio haloes and with theoretical expectations of the reacceleration/turbulence scenario;
- A1351 is a very complex cluster, with two main subclusters projected in the northern region and connected with the two peaks in the velocity distribution, and other minor substructures, all tracing the N–S cluster elongation.

Therefore, we conclude that in the above scenario, the quite peculiar, diffuse radio emission can be reduced to a much more typical emission (halo plus relic), strongly supporting a previous suggestion based only on the inspection of radio data and preliminary X-ray data. We stress, however, that the study of so complex a cluster would be greatly advantageous with a substantial improvement of data. A much larger redshift dataset would allow the detection of individual subcluster cores. In addition, deeper X-ray observations would make it possible to construct X-ray temperature and metallicity maps.

More generally, considering our previous results about structure of DARC clusters, we conclude that peculiar features in the diffuse radio emission could be interpreted by considering the details of the complex cluster structure, for instance in Abell 520, hosting a very elongated radio halo (Girardi et al. 2008), and in Abell 2345, hosting two quite asymmetric radio relics (Boschin et al. 2010). In this context, the study of the galaxy kinematics represents an important ingredient, critical to our understand of the geom-

etry of the merger and to detecting possible LOS aligned substructures.

ACKNOWLEDGEMENTS

We are indebted to Tiziana Venturi for the VLA radio image. RB acknowledges financial support from the Spanish Ministry of Economy and Competitiveness (MINECO) under the 2011 Severo Ochoa Programme MINECO SEV-2011-0187. MG acknowledges financial support from MIUR PRIN2010-2011 (J91J12000450001). This publication is based on observations made on the island of La Palma with the Italian Telescopio Nazionale Galileo (TNG) and the Isaac Newton Telescope (INT). The TNG is operated by the Fundación Galileo Galilei – INAF (Istituto Nazionale di Astrofisica). The INT is operated by the Isaac Newton Group. Both telescopes are located in the Spanish Observatorio del Roque de Los Muchachos of the Instituto de Astrofisica de Canarias. This research has made use of the NASA/IPAC Extragalactic Database (NED), which is operated by the Jet Propulsion Laboratory, California Institute of Technology, under contract with the National Aeronautics and Space Administration.

REFERENCES

Abell G. O., Corwin H. G. Jr., Olowin R. P., 1989, ApJS, 70, 1
Allen S. W., Schmidt R. W., Fabian A. C., Ebeling H., 2003, MNRAS, 342, 287
Arnaud K. A., 1996, in "Astronomical Data Analysis Software and Systems V" (eds. G. Jacoby and J. Barnes), ASP Conf. Ser., 101, 17
Ashman K. M., Bird C. M., Zepf S. E., 1994, AJ, 108, 2348
Basu K., 2012, MNRAS, 421, L112
Beers T. C., Flynn K., & Gebhardt K. 1990, AJ, 100, 32
Beers T. C., Geller M. J., Huchra J. P., 1982, ApJ, 257, 23
Bertin E., Arnouts S., 1996, A&As, 117, 393
Bird C. M., Beers T. C., 1993, AJ, 105, 1596
Böhringer H., Voges W., Huchra J. P., et al., 2000, ApJS, 129, 435
Boschin W., Girardi M., Barrena R., 2013, MNRAS, 434, 772
Boschin W., Girardi M., Barrena R., et al., 2004, A&A, 416, 839
Boschin W., Barrena R., Girardi M., 2010, A&A, 521, A78
Boschin W., Girardi M., Barrena R., Nonino M., 2012, A&A, 540, A43
Brunetti G., Cassano R., Dolag K., Setti G., 2009, A&A, 507, 661
Brunetti G., Setti G., Feretti L., Giovannini G., 2001, MNRAS, 320, 365
Brunetti G., Venturi T., Dallacasa D., Cassano R., Dolag K., Giacintucci S., Setti G., 2007, ApJ, 670, L5
Buote D. A., 2002, in Feretti L., Gioia I. M., Giovannini G., eds., Merging Processes in Galaxy Clusters, Kluwer, Dordrecht, p. 79
Cassano R., Brunetti G., Setti G., 2006, MNRAS, 369, 1577
Cassano R., Brunetti G., Venturi G., et al., 2008, A&A, 480, 687
Cassano R., Ettori S., Giacintucci S., Brunetti G., Markevitch M., Venturi T., Gitti M., 2010, ApJl, 721, 82
Cavaliere A., Fusco-Femiano R., 1976, A&A, 49, 137
Dahle H., Kaiser N., Irgens R. J., Lilje P. B., Maddox S. J., 2002, ApJS, 139, 313
Danese L., De Zotti C., di Tullio G., 1980, A&A, 82, 322
De Grandi S., Molendi S., 2009, A&A, 508, 565
den Hartog R., Katgert P., 1996, MNRAS, 279, 349
Dressler A., Shectman S. A., 1988, AJ, 95, 985
Ensslin T. A., Biermann P. L., Klein U., Kohle S., 1998, A&A, 332, 395
Ensslin T. A., Gopal-Krishna, 2001, A&A, 366, 26
Ensslin T. A., Pfrommer C., Miniati F., Subramanian K., 2011, A&A, 527, A99
Fadda D., Girardi M., Giuricin G., Mardirossian F., Mezzetti M., 1996, ApJ, 473, 670
Fasano G., Franceschini A., 1987, MNRAS, 225, 155
Feretti L., Giovannini G., Govoni F., Murgia M., 2012, A&ARv, 20, 54
Ferrari C., Maurogordato S., Cappi A., Benoist C., 2003, A&A, 399, 813
Ferrari C., Govoni F., Schindler S., Bykov A. M., Rephaeli Y., 2008, Space Sci. Rev., 134, 93
Giacintucci S., Venturi T., Cassano R., Dallacasa D., Brunetti G., 2009, A&A, 704, L54
Giovannini G., Bonafede A., Feretti L., et al., 2009, A&A, 507, 1257
Giovannini G., Feretti L., 2002, in Feretti L., Gioia I. M., Giovannini G., eds., Merging Processes in Galaxy Clusters, Kluwer, Dordrecht, p. 197
Girardi M., Bardelli S., Barrena R., Boschin W., Gastaldello F., Nonino M., 2011, A&A, 536, A89
Girardi M., Barrena R., Boschin W., 2010, Contribution to the conference "Galaxy clusters: observations, physics and cosmology", p.38
Girardi M., Barrena R., Boschin W., Ellingson E., 2008, A&A, 491, 379
Girardi M., Biviano A., 2002, in Feretti L., Gioia I. M., Giovannini G., eds., Merging Processes in Galaxy Clusters, Kluwer, Dordrecht, p. 39
Girardi M., Borgani S., Giuricin G., Mardirossian F., Mezzetti F., 2000, ApJ, 530, 62
Girardi M., Boschin W., Barrena R., 2010, A&A, 517, 65
Girardi M., Escalera E., Fadda D., Giuricin G., Mardirossian F., Mezzetti M., 1997, ApJ, 482, 41
Girardi M., Fadda D., Giuricin G., Mardirossian F., Mezzetti, M., Biviano, A., 1996, ApJ, 457, 61
Girardi M., Giuricin G., Mardirossian F., Mezzetti M., Boschin W., 1998, ApJ, 505, 74
Girardi M., Mezzetti M., 2001, ApJ, 548, 79
Govoni F., Ensslin T. A., Feretti L., Giovannini G., 2001, A&A, 369, 441
Hoeft M., Brüggen M., Yepes G., 2004, MNRAS, 347, 389
Holhjem K., Schirmer M., & Dahle H., 2009, A&A, 504, 1
Irgens R. J., Lilje P. B., Dahle H., Maddox S. J., 2002, ApJ, 579, 227
Kalberla P. M. W., Burton W. B., Hartmann D., et al., 2005, A&A, 440, 775 (LAB Map)
Leccardi A., Molendi S., 2008, A&A, 486, 359
Lopes P. A. A., de Carvalho R. R., Kohl-Moreira J. L., Jones C., 2009, MNRAS, 399, 2201
Markevitch M., Gonzalez A. H., David L., Vikhlinin A.,

Murray S., Forman W., Jones C., Tucker W., 2002, ApJ, 567, L27
Maurogordato S., Sauvageot J. L., Bourdin H., Cappi A., Benoist C., Ferrari C., Mars G., Houairi K., 2011, A&A, 525, A79
Owen F., Morrison G., Voges W. 1999, proceedings of the workshop "Diffuse Thermal and Relativistic Plasma in Galaxy Clusters", eds. H. Böhringer, L. Feretti, & P. Schuecker, MPE Report 271, pp. 9–11
Patel S. K., Joy M., Carlstrom J. E., et al., 2000, ApJ, 541, 37
Pisani A., 1993, MNRAS, 265, 706
Pisani A., 1996, MNRAS, 278, 697
Popesso P., Biviano A., Böhringer H., Romaniello M., Voges W., 2005, A&A, 433, 431
Roettiger K., Burns J. O., Stone J. M., 1999, ApJ, 518, 603
Roettiger K., Loken C., Burns J. O., 1997, ApJS, 109, 307
Rossetti M., Eckert D., Cavalleri B. M., Molendi S., Gastaldello F., Ghizzardi S., 2011, A&A, 532, 123
Schuecker P., Böhringer H., Reiprich T. H., & Feretti L., 2001, A&A, 378, 408
Serna A., Gerbal D., 1996, A&A, 309, 65
Serra A. L., Diaferio A., 2013, ApJ, 768, 116
Thompson L. A., 1982, in Early Evolution of the Universe and the Present Structure, Proc. IAU Symp. 104, Abell G. O., Chincarini G., eds., Reidel, Dodrecht, p. 63
Tonry J., Davis M., 1979, AJ, 84, 1511
Venturi T., Giacintucci S., Macario G., et al., 2008, A&A, 484, 327
Venturi T., 2011, Mem. Soc. Astron. Italiana, 82, 499
West M. J., Bothun G. D., 1990, ApJ, 350, 36